POLITECNICO DI TORINO
Repository ISTITUZIONALE

An advanced post-necking analysis methodology for elasto-plastic material models identification

(Article begins on next page)
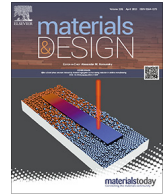
27 April 2024

An advanced post-necking analysis methodology for elasto-plastic material models identification

Marta Beltramo *, Martina Scapin, Lorenzo Peroni

Politecnico di Torino, Department of Mechanical and Aerospace Engineering, Corso Duca degli Abruzzi, 24, 10129 Turin, Italy

HIGHLIGHTS

- An alternative hybrid methodology which combines a FE-based inverse method with a 1D description of necking is proposed.
- The procedure identifies the plastic flow curve starting from the measurement of the specimen profile in one deformed configuration.
- The adoption of a piecewise plasticity model allows to accurately describe the uniform phase and the necking onset.
- The proposed strategy was proved to be adequate for reproducing the post-necking behavior of metallic materials.

GRAPHICAL ABSTRACT
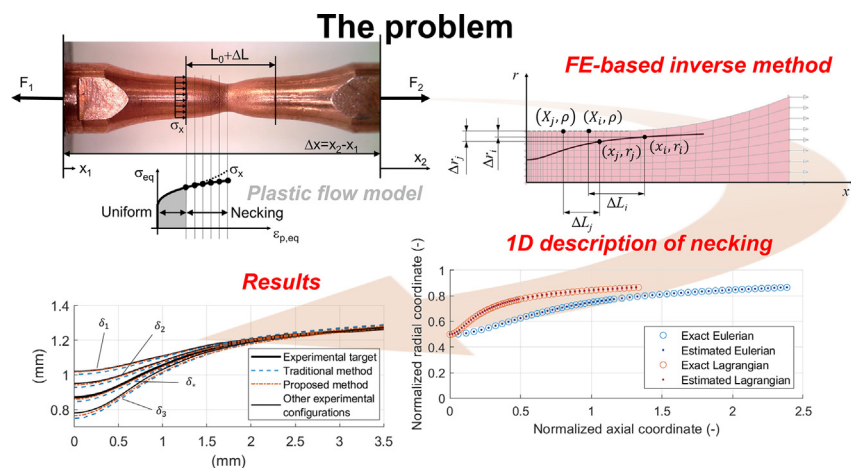
ARTICLE INFO

ABSTRACT

The tensile test is widely used for identifying the material plastic flow curve: this is a fundamental step in the design and in material behavior analysis. However, during these tests on ductile metals the necking phenomenon occurs, and the stress and strain states become triaxial and non-uniform. In the scientific literature several characterization methods have been proposed to properly address these aspects.

The present work proposes an alternative strategy for identifying the plastic flow curve, focusing on temperature and strain-rate insensitive elasto-plastic materials. This is a hybrid methodology whereby a FE-based inverse method is combined with the 1D description of necking proposed by Audoly and Hutchinson. Indeed, the inverse method employs as target function the specimen profile, but to properly define it a relationship between the original and the deformed configuration of the tensile sample is required, and it is provided by this 1D model.

The accuracy and the validity of the proposed strategy was verified on benchmark cases with ad-hoc experimental profiles obtained via numerical simulations. Finally, this method was applied to real case studies and the identified plastic flow curve was compared with the one obtained using a traditional FE-based inverse method having as target the force-stroke curve.

© 2023 The Author(s). Published by Elsevier Ltd. This is an open access article under the CC BY-NC-ND license (http://creativecommons.org/licenses/by-nc-nd/4.0/).

---

* Corresponding author.
    E-mail address: marta.beltramo@polito.it (M. Beltramo).

1. Introduction

Currently, finite element (FE) simulations are widely used in many fields, from research to product and process design. One essential aspect for the reliability of the results is the material constitutive law, for what it concerns both the mathematical model and the parameters. Indeed, these latter often require a calibration starting from experimental data to adequately represent the response of the material to the stresses that are of interest.

Particularly, the determination of the plastic flow curve for a metallic material implies in most cases to perform tensile tests. This testing methodology has some uncontested advantages with respect to other tests: indeed, it is easy to be performed, the force is uniaxial, high levels of plastic strain can be induced and can also bring the material to fracture. For these reasons, it is the main test among all the possible mechanical ones which can be coupled with non-standard environment conditions (in terms of temperature, corrosion, etc.) and which can be performed at different strain-rates (exploiting the dependence from quasi-static to high dynamic conditions).

Regardless of the specific testing conditions, the aim of the experimenter is to obtain the values of equivalent stress and equivalent strain which develop in the specimen during the whole test, starting from experimental measurements.

Nowadays, there are several techniques which allow the local or global measurement of the deformation (strain-gages, extensometers, Digital Image Correlation analysis, etc.). The evaluation of the specimen deformation directly from the displacement of the crosshead of the testing machine does not provide acceptable results. This is due to the well-known problem related to the deformability of the testing machine: indeed, this can be higher than that of the specimen itself and may require the identification and application of a correction factor to the measurements. Unfortunately, there is no other possibility for directly evaluating the stress except to derive it from the force applied to the specimen.

By supposing to overcome the above-mentioned problems and to be able to obtain the equivalent stress vs. equivalent strain curve from the results of a mechanical test, the next step would be fitting these data with a mathematical model to be used in FE codes.

If the specimen exhibits uniform deformation inside its gauge length, the identification of the equivalent stress vs. equivalent strain curve is easy and immediate. Indeed, knowing the longitudinal stress and strain (x direction) inside the specimen, the equivalent values can be determined as reported in Eq. (1):

$$\sigma_{eq} \equiv \sigma_x \text{ and } \varepsilon_{eq} \equiv \varepsilon_x. \tag{1}$$

Nevertheless, during a tensile test of a ductile metallic material, it is almost impossible that the instability condition is not reached. On the basis of Considère's criterion, the necking occurs when:

$$\frac{dF}{d\varepsilon} = 0 \rightarrow \frac{d\sigma}{d\varepsilon} = \sigma. \tag{2}$$

Hence the necking phenomenon can be considered a characteristic of the material, depending on its hardening behavior. Therefore, known the plastic flow curve, the level of deformation at which necking occurs can be determined using Eq. (2). However, it is not possible to predict the section in which the deformation will localize (this actually depends on the inhomogeneity of the material, roughness of the specimen, inaccuracies in its metal working, etc.). The fact that it is not possible to predict the section in which necking will occur leads to the conclusion that this represents a problem of instability and bifurcation and, indeed, later works with respect to Considère studied the phenomenon by means of the so-called "bifurcation theory" [1–3].

With reference to the scheme of Fig. 1, during a tensile test, the displacements imposed to the heads of the specimen (x_1 and x_2)

produce an elongation Δx of the specimen which opposes the deformation generating forces (F_1 and F_2). During a quasi-static test or when the equilibrium is established in a dynamic one, the forces at the two sides are equal and depend on Δx history. In a uniform regime, the stress state is uniaxial, and the induced axial stress (σ_x) is equal to the equivalent stress (σ_{eq}).

According to Considère's criterion, when the condition defined by Eq. (2) is satisfied there is the onset of necking, and the deformation starts to localize inside the specimen. In this phase of the test, the sample assumes the typical shape reported in Fig. 1, which is characterized by triaxial and non-uniform states of stress and strain. The axial stress is no longer the unique component of stress and is higher than the equivalent stress.

Therefore, the proper determination of the post-necking flow stress curve starting from the experimental data of a tensile test would require the evaluation of all the stress and strain components for the definition of the yielding surface and its strain/time evolution (hardening law).

The simplest strategy that is sometimes adopted to determine the post-necking behavior consists of fitting with a hardening model the experimental data before the necking onset and then extrapolating the plastic flow curve for higher levels of strain. However, this can lead to very different results depending on the mathematical model chosen [4–6]. Indeed, it is not advisable to use a model for studying deformations higher than those considered for the development of the model itself. This is a problem especially for almost perfectly plastic materials: since necking occurs as soon as they enter the plastic regime, the hardening law would be based on the few experimental data that precede necking and which could be highly affected by measurement uncertainties (as they derive from measurements of small displacements).

An adequate identification of the plastic behavior for strains higher than the one at which necking occurs, is of great importance because different applications (such as forming, dynamic impact processes, energy absorbers, etc.) require the materials to undergo a higher level of deformation. So, in order to continue to exploit the advantages of the uniaxial tensile test, for decades researchers proposed several methodologies of analysis for evaluating the stress and strain components during the necking and for the identification of the relationship between them in the plastic domain.

The most famous work for evaluating the stress components during necking is for sure Bridgman's theory [7], which proposed a theoretical solution of this problem based on the neck geometry and some strong simplifying assumptions. Bridgman's correction factor of the average axial stress requires the accurate measurement of the curvature and the minimum radius in the neck section during the tensile test.

Starting from his work, several other theories and models were proposed with the aim to improve or partially modify it [8]. The main problem related with this approach is determining the curvature, since it requires to acquire and elaborate images during the test to extract the profile, which then has to be fitted with a mathematical function. In [9], the curvature in the necking region was related to the difference between the actual strain and the strain at the necking onset. In [10], to overcome the problem related with the determination of the curvature, a modified version of Bridgman's theory was obtained, whereby the correction factor only depended on the radius of the minimum cross-section. In [11], a material-independent correction factor was found, which should be able to correct the stress vs. strain curve after necking, reducing the error with respect to Bridgman's theory. This was employed in later studies [12] and extended to high strain-rates [13]. In addition to the previous methods, some researchers derived the correction factors and formulae with numerical tensile modeling. This strategy consists of performing numerical tensile tests with prede-
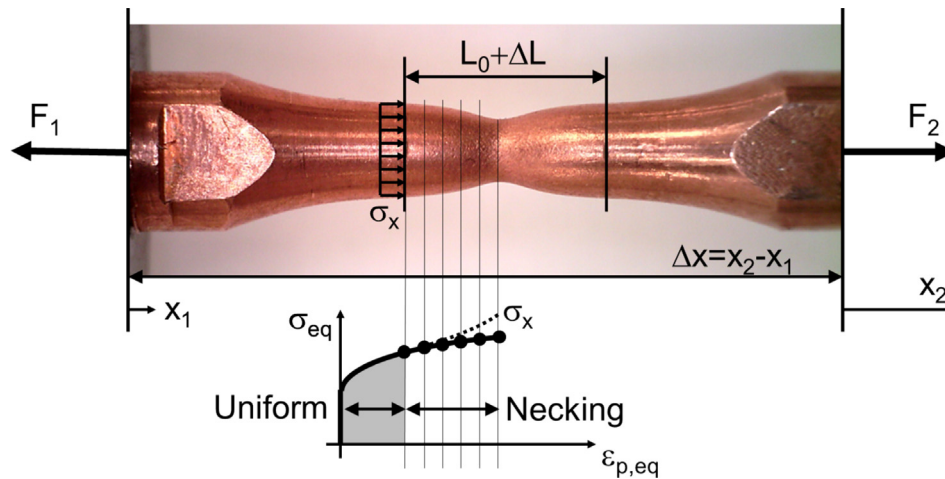
Fig. 1. Scheme of force and displacement applied to a specimen during a tensile test. Comparison between axial and equivalent stress in uniform and necking phases as a function of the equivalent plastic strain.

fined equivalent stress vs. strain curve and searching for a formula that fits the relationship between the true stress from numerical simulations and the input equivalent stress at the same equivalent strain [14,15]. A similar approach was adopted in [16] to determine a function which relates the material hardening behavior with the initial geometry of a notched specimen and the final radius of the minimum cross-section. The main issue of these methodologies is that a preselected hardening law is assumed, but actually each material exhibits a specific hardening rule, so the accuracy of these correction factors cannot be guaranteed.

Moreover, it is noteworthy, for analyzing the main aspects of necking, the development of 1D models describing the phenomenon. A first important contribution is that from Mielke [17], who properly derived the 1D model through a dimensional reduction of 2D and 3D continuum mechanics. Later on, this work was extended by Audoly and Hutchinson [2]: the necking phenomenon is seen as a bifurcation state from a condition of uniform deformation and the dimensional reduction applied to a prismatic solid leads to a 1D energy functional able to describe necking. This model was further extended to rate-dependent materials in [18].

Alternatively, thanks to the increasing spread of nonlinear FE codes and the higher computational power availability, many researchers exploited FE analysis to investigate the necking phenomenon and computing the triaxial state of stress and strain.

The FE analysis requires the definition of a proper constitutive equation of the material. The identification of the model parameters is mainly related to the capability to find an adequate method for fitting the experimental data and the capability to identify which are the best or more convenient experimental data to use. For the fitting procedure very efficient algorithms are available and can be easily implemented.

Numerical inverse methods based on FE simulations were widely used to identify the plastic flow curve. Many methodologies can be applied, but the main advantage with respect to the previously reported techniques is that it is not necessary to compute a correction factor or to determine the equivalent stress vs. equivalent plastic strain from the experimental test. Indeed, the inverse method directly compares experimental and numerical results. This comparison is done by defining objective or target functions, which are correlated to quantities experimentally measurable during the test. Regardless of the optimization algorithm and strategy, the basic principle is to optimize the set of the unknown model parameters by starting from a trial set of values and trying different combinations in order to satisfy the imposed requirements and

constraints of the target function. A widespread approach is to use macroscopic quantities, such as the force vs. displacement curve obtained from the test [19–23], or the experimental force vs. diameter reduction curve [24]. Sometimes the validation of this type of procedure was performed by comparing the obtained deformed shape of the specimen (or at least the minimum diameter), during necking or as post-mortem analysis. This was done at the end of the optimization procedure, without considering the necking profile as one of the objective functions of the inverse method based on FE simulations [25–29].

In other cases, information coming from full-field measurements is used as objective function. In a lot of works the Digital Image Analysis was applied to measure the plastic strain on the surface or in some specific points [30–35]. The information coming from full-field measurements (in terms of strain or displacement fields) was used as target function in addition to the force time history in inverse numerical approaches for the identification of the flow stress curve [36–38].

In some cases, full-field measurements were used within an optimization technique that did not exploit FE simulations, but was based on the Virtual Field Method: the objective function was the minimization of the error between internal and external work, as proposed in [4] and validated in [39], under the principle that the internal work, which is correlated to stress, can be obtained from the strain measurement.

Furthermore, hybrid methods which combine the FE-based numerical inverse procedure with other methodologies were proposed too. In [40] a method combining FE analysis and hybrid particle swarm optimization was proposed in order to determine the yield curve of round rod after necking. In [41] curve fitting was used to obtain the hardening model before necking, whereas FE-based inverse method was employed to predict the post-necking curve.

In the present work, starting from quasi-static tensile tests at room temperature, a mixed methodology for material model parameters identification was proposed. The experimental measurement of the necking profile was used as the target in the inverse method based on FE simulations and combined with Audoly and Hutchinson's results [2], to correctly establish a relationship between the original configuration of the specimen and the deformed one. A more extended description of the model proposed by [2] is discussed in the next section, mainly highlighting the results used in the present approach.

The new methodology proposed is compared with a traditional numerical inverse method based on the comparison of the force vs. stroke curve. These two methods are independent of each other, so the authors investigated the potential of using both methods to increase the reliability in the identification of the hardening law.

The model proposed in [2] is also able to determine the response of an elasto-plastic material, given its flow stress curve, but this problem is intrinsically incremental. Hence, in order to use this 1D model to characterize elasto-plastic materials an optimization would be required, and the resulting identification methodology would represent an inverse numerical method based on a 1D model. However, as already mentioned, the approach followed in the present work is an inverse method based on FE simulations, which exploits some of the results of the 1D theory proposed in [2].

In general, a critical issue in material characterization is the choice of the material model. This is because if the model was not suitable and did not correctly take into account all the variables of the problem (such as strain, strain-rate and temperature), the solution obtained would not be adequate, regardless of the identification method used. Thus, over the last decades a high number of strength material models for the mathematical description of the yield surface has been developed and implemented.

In this work, among the most widespread hardening models implemented in many FE codes, the following were employed: power-law (also known as the Hollomon or Ramberg-Osgood model) [42,43], Johnson-Cook [44] and Voce [45]. In addition, the use of a piecewise linear hardening law is analyzed too: indeed, since in this case there is no specific mathematical relationship between equivalent stress and equivalent plastic strain, it is possible to better describe the behavior of a material [30,36,46,47].

The formulations used are the simplified ones, in which temperature and strain-rate are not taken into account. Indeed, since approaches based on the profile analysis are not very common, it is necessary to study their potential in a condition without thermal and strain-rate effects. Therefore, the present investigation focuses on materials which are not very sensitive to these variables and on test conditions such that the material is loaded isothermally and with a negligible effect of strain-rate. However, temperature and strain-rate would not modify the validity of the procedure, but they would increase the level of complexity of the results explanation and prevision and require future detailed studies not taken on in this preliminary work.

1.1. 1D model for necking analysis

The model proposed in [2] is able to predict the necking localization for nonlinear materials, being an interesting and valid alternative to 2D and 3D approaches. In [2], the 1D model was derived for prismatic solids having an arbitrary cross-section (see Fig. 2a) and made of hyperelastic material, taking into account orthotropy and compressibility; then it was applied to 2D blocks (plain strain) or round bars (axial-symmetry, see Fig. 2b) introducing also the hypothesis of isotropy and incompressibility. Such model was then modified to account for the elastic unloading typical of elasto-plastic materials; this was accomplished by considering that the unloading starts far from the center of the neck and propagates towards it.

The theory provides a 1D description of the problem, that, unlike many other 1D models, is asymptotically correct (i.e., for $D/L \rightarrow 0$) because it has been derived through a rigorous dimensional reduction. Moreover, this is a Lagrangian description of the necking phenomenon, since all the quantities are computed referring to a reference configuration.

Considering as reference configuration the undeformed one, the cross-sections are perpendicular to the axis, so the X coordinate is enough to identify their position. On the other hand, in the deformed configuration the cross-sections become curved, thus it is convenient to refer to their average longitudinal position $\Lambda(X)$, which is calculated as the average of the longitudinal positions (x) of all the points that belonged to that section X in the undeformed configuration. By deriving $\Lambda(X)$, the longitudinal stretch $\lambda(X)$ is obtained, which is the main independent variable of the 1D theory:

$$\lambda(X) = \frac{d\Lambda(X)}{dX} \tag{3}$$

Of course, as long as the deformation is uniform, all the sections move proportionally to their initial position and therefore the longitudinal stretch is constant. While, from the necking onset, the deformation localizes and consequently $\lambda(X)$ is higher closer to the minimum cross-section. This is shown in Fig. 3.

The main kinematic result of Audoly and Hutchinson's theory [2], applied to a orthotropic solid having an arbitrary cross-section, is that the deformed coordinates $x = (x, y, z)$ of a point of initial coordinates $\underline{X} = (X, Y, Z)$ can be determined as:

$$x\left(\underline{X}\right) = \Lambda(X) + \frac{d\lambda}{dX}(X)c(\lambda(X))\left(\frac{Y^2 + Z^2}{2} - \frac{I}{2A_0}\right),$$
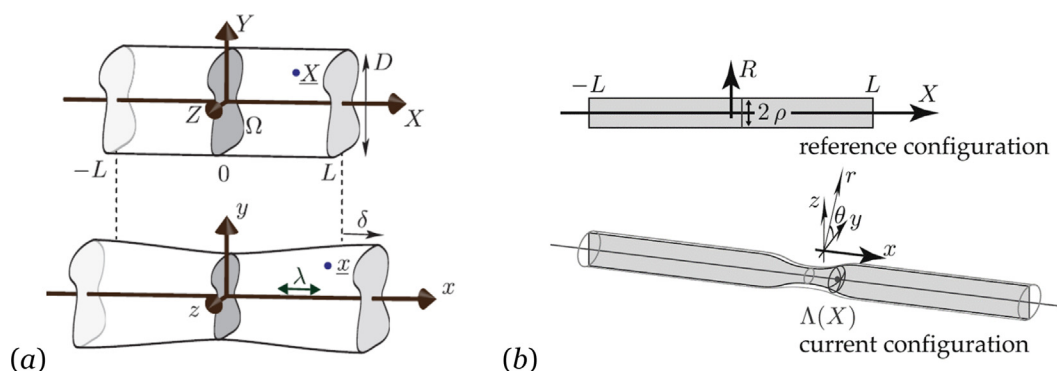
Fig. 2. Problem definition and comparison between reference and deformed configuration. $X = (X, Y, Z)$ represents the position of a point belonging to a general cross-section in the reference configuration, $x = (x, y, z)$ represents the position of the same point in the current configuration. (a) Solid having an arbitrary cross-section: D represents the dimension of the cross-section and L the axial portion taken into account [2]. (b) Cylinder with length 2L and radius ρ [18].

Fig. 3. Comparison of mean axial position and axial stretch for a configuration in uniform deformation and one in the necking phase.

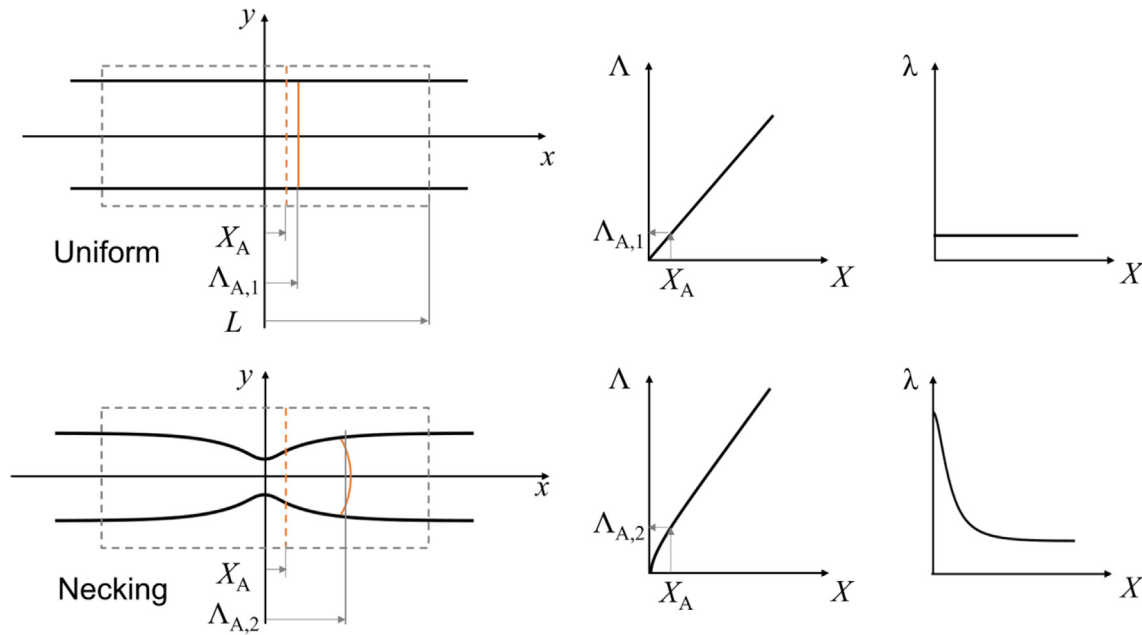$$y\left(\underline{X}\right) = \mu_0(\lambda(X))Y,$$

$$z\left(\underline{X}\right) = \mu_0(\lambda(X))Z, \tag{4}$$

where $\mu_0(\lambda(X))$ represents the transverse stretch as a function of the longitudinal stretch, $c(\lambda(X))$ is the curvature coefficient defined as: $c(\lambda) = -\frac{\mu_0}{\lambda}\frac{d\mu_0}{d\lambda}$, I is the geometric moment of inertia of the cross-section, A_0 is the undeformed cross-sectional area.

Therefore, the longitudinal position depends on the average displacement of the section and its curvature, whereas the transversal position depends on the transversal stretch related to the Poisson effect.

A simpler case with respect to the general one presented in Eq. (4) can be considered hereinafter. Indeed, the portion of a dog-bone cylindrical specimen which is taken into account for the analysis of the tensile test is the gauge length, that is actually a round bar. Moreover, the material between the shoulders and the part of reduced section guarantees uniaxial stress in the gauge length (as long as the deformation is uniform); thus, if the material has an isotropic behavior, the portion considered is undergoing axisymmetric deformation. Hence the problem becomes the one of a round bar of initial radius ρ and initial length $2L$ undergoing axisymmetric deformation, which actually represents a 2D problem. In particular, X and R are respectively the axial and radial directions (Fig. 2b).

According to the results presented in [2] and considering the material isotropic and incompressible, for the 2D axisymmetric problem, the deformed coordinates (x, r) of a point of initial coordinates (X, R) become:

$$x(X, R) = \Lambda(X) + \frac{1}{4\lambda(X)^3}\frac{d\lambda(X)}{dX}\left(R^2 - \frac{\rho^2}{2}\right), \tag{5a}$$

$$r(X, R) = \frac{R}{\sqrt{\lambda(X)}}. \tag{5b}$$

These relationships are of great importance for the method proposed in this paper since they also allow, starting from a deformed specimen profile, to determine the original position of the points on the external surface. This aspect will be described in detail in the following section.

2. Proposed method

The aim of the present work is to propose and evaluate a new possible method for the identification of the plastic flow curve, exploiting an inverse approach based on FE simulations and having as target function the specimen profile in the necking region for axisymmetric specimens.

In a cylindrical specimen, if the material has an isotropic behavior, the axisymmetric geometry is maintained also during the necking phase. It means that the external surface is axisymmetric and that the external profile can be determined from the analysis of 2D images obtained with a video camera.

Also in [48–50] researchers proposed methods of identification of the plastic flow curve based on the analysis of the specimen shape; these strategies were later used in [51,52]. The methodologies presented in [48,50] employed FE simulations and optimization techniques for determining and minimizing an objective function which took into account the displacements of few points on the specimen surface. Instead, in [49] an expression for a correction factor of the stress was theoretically determined as a function of the strains.

However, the relationships used in [49], had some approximations: they propose to evaluate the axial stress on the external surface in the neck cross-section, by imposing that the radial and the circumferential stresses are both zero, which generally is not valid in the necking region. Therefore, in order to not introduce such simplifying hypothesis, the approach proposed in the present paper exploits FE simulations to calculate stress and strain distributions.

Moreover, the aim of the authors is to avoid performing measurements on the specimen surface by using marker, speckle or deposited pattern, which are used in the methods proposed by [48–50] and which in general are required by Digital Image Correlation or Digital Image Analysis techniques. Indeed, painting the surface and recording it by means of a high speed/resolution camera could be difficult or even impossible in some conditions, such as at high temperature (in which the paint could not be applicable

at all or visible after the heating) and/or at high strain-rate (in which the layer can be detached from the specimen surface). In addition, due to the high levels of deformation which can be reached during necking in a metallic material (even about 400%), the painted layer could be affected by heavy problems and would no longer give reliable results.

According to the goal to find a method applicable in all the testing conditions, the measurement of the reduction of the external diameter is performed. This is a superficial quantity, and it is also non-uniformly distributed along the axis of the specimen during the necking phase, hence it is not possible to directly evaluate neither the effective plastic strain nor the equivalent stress. In any case, the radial coordinates measured at different longitudinal coordinates (i.e., the distribution on the surface of the circumferential strain) can be used as target function in an inverse procedure.

2.1. Correlation between flow stress curve and deformed shape during necking

Before going into details of the implementation of the proposed methodology, it is necessary to highlight the correlation between the flow stress curve and the deformed shape during necking.

At first, some considerations can be made, using for example FE simulations. Six points on the external surface of the specimen were chosen (points A, A_1, A_2, B, C, D in Fig. 4); they were not equally spaced in the undeformed configuration in order to have more points in the region close to the section where necking would occur.

It is possible to verify that all material points follow the same hardening curve simultaneously as long as the deformation is uniform. It means that the histories of the equivalent stress and equivalent strain are the same whatever point is considered. However, the necking onset gives rise to triaxiality and localized deformation, so that the material points that have not been reached by the unloading boundary yet continue to follow the same hardening law, but at a different rate with respect to each other. More specifically, in the necking region the temporal evolution is faster and therefore, at a given time, the level of strain reached is higher than elsewhere. In the meantime, the elastic unloading gradually moves towards the mid minimum cross-section of the specimen and

when a material point is reached by the unloading boundary, it turns back in the elastic field. Actually, the stress decreases up to a certain level, such that the equilibrium is guaranteed, while the plastic equivalent strain remains constant (see Fig. 4a). As a consequence, each point keeps memory of the level of strain reached and the radial coordinate of the portion of the specimen outside the necking region gives information about the maximum uniform strain (the one just before the necking onset).

To conclude, each point of the surface of the specimen is characterized by specific values of circumferential, radial, and axial strain. Since each strain state is caused by the different state of stress developed depending on the longitudinal position with respect to the minimum section, each point is representative of a different portion of the hardening curve [53].

Therefore, once the instability has been overcome, a single deformed configuration is sufficient to provide the necessary information for describing the entire flow stress curve up to the reached level of strain. Actually, this allows to determine the shape of the flow stress curve, since scaled curves lead to the same specimen profile, whereas in order to get a unique law, additional information about the level of stress is required.

Before the instability condition is reached, the deformation of the specimen is uniform: hence the deformed profile cannot be used to extract information on the hardening law. The only information which can be derived is the amount of equivalent plastic strain from the measurement of the circumferential strain, because in this phase it is correct that:

$$\varepsilon_{eq} = \varepsilon_x = -2\varepsilon_c \quad \text{and} \quad \sigma = \frac{F}{A} \tag{6}$$

Moreover, it is possible to determine the actual area A and compute the stress starting from the measurement of the force. Such a stress gives a correct evaluation of σ_{eq}.

On the basis of these considerations, in the present work the authors propose to identify the plastic flow curve through an inverse numerical method that uses as target a post-necking deformed shape at a certain time instant. The outputs of the methodology are both the plastic flow curve and also the engineering curve. Instead, the traditional approach uses as target the engineering curve (or equivalently the force vs. stroke curve), so the
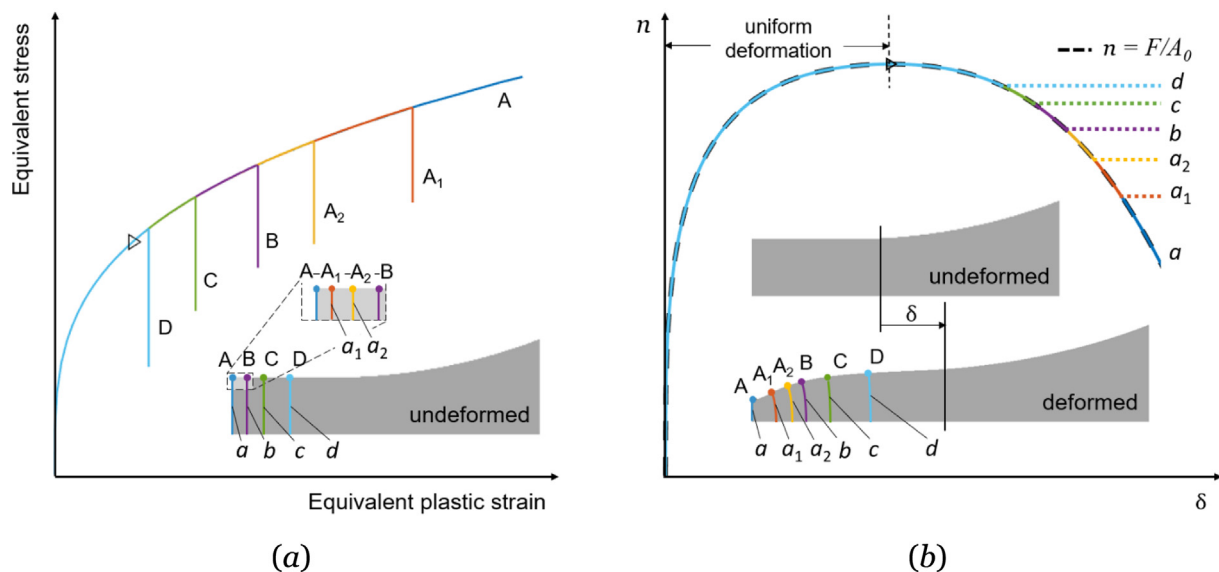
Fig. 4. (a) Equivalent stress vs. equivalent plastic strain for different points on the external surface of the specimen. (b) Engineering (or nominal) stress vs. half elongation of the gauge length; each curve (except for the dashed one) is obtained by applying Eq. (7) to the corresponding section. The points and the sections considered are shown in the undeformed configuration on the left plot and in a deformed configuration on the right plot. The triangle represents the necking onset.

time evolution of the system. In this case the plastic flow curve and the deformed shape are obtained as results of the optimization procedure.

A mathematical relationship between the material constitutive law, the engineering stress and the deformed shape is provided by the 1D theory of Audoly and Hutchinson [2] for a hyperelastic material:

$$\frac{dw_0}{d\lambda}(\lambda) - 2\rho^2 \frac{db}{d\lambda}(\lambda)\left(\frac{d\lambda}{dX}\right)^2 - 4\rho^2 b(\lambda)\frac{d^2\lambda}{dX^2} = n, \tag{7}$$

where n is the engineering (or nominal) stress, w_0 is the strain energy density in case of uniform deformation and b is a modulus associated with the regularizing second gradient of the strain. The latter two are both function of λ and depend on the geometry, the loading condition and the material law. In this case of axisymmetric deformation of a round bar:

$$b(\lambda) = \frac{1}{32\lambda^4}\frac{dw_0}{d\lambda}. \tag{8}$$

Writing Eq. (7) for the section $X = 0$ (section a in Fig. 4), an expression formally analogous to that of Bridgman [7] is obtained, allowing to evaluate the engineering curve through the time evolution of the central section.

From a physical point of view, n is only function of time, so Eq. (7) applied to different sections X at the same time t should give the same result. This is respected during uniform deformation: indeed, before necking, at a specific time, Eq. (7) leads to the same n at every X (this because $\lambda(X)$ is constant); this value of n is also in agreement with the one computed as F/A_0.

At the necking onset, the unloading boundary is generated, but Eq. (7), which was obtained for a hyperelastic material, does not consider the unloading typical of elasto-plastic materials. This implies that Eq. (7) is no more valid for those sections X that have undergone unloading. So, considering a specific section X, the consequence is: before section X is reached by the unloading boundary, n computed through Eq. (7) is in agreement with the engineering stress F/A_0; starting from the time in which that section X is reached by the unloading boundary, λ, $\frac{d\lambda}{dX}$, $\frac{d^2\lambda}{dX^2}$ remain constant in time (no more deformation is done, once unloading occurred), therefore Eq. (7) gives a value of n (on that section) which remains constant in time at the value it had when unloading took place.

The results for the sections a, a_1, a_2, b, c, d are reported in Fig. 4b. Each section is associated with a color, that is the same used in Fig. 4a for the point which belongs to that section and which is on the specimen surface. The colored line is continuous before that section is reached by the unloading boundary and then it becomes a dotted line.

Therefore, given a specific deformed configuration and applying Eq. (7) to all the sections, the ones that are in the plastic field give all the same engineering stress value, while those that have already undergone elastic unloading give a different value, which represents the engineering stress when the unloading boundary reached each section (see Fig. 4b). If it was possible to determine when the unloading took place in each section, then the engineering curve could be obtained from a single profile. By means of the 1D model proposed in [2] it would be possible to determine the engineering strain at which a specific section is unloaded. However, since the methodology employed in the present paper exploits FE simulations, these aspects of the 1D theory are not directly necessary, but they allow to establish, known the material, a correlation between the engineering curve and the deformed profile for a quasi-static case like the one here analyzed.

In conclusion, considering that the engineering curve (or equivalently the force vs. stroke curve) is widely used to identify the

plastic flow curve by an inverse numerical method, then a correlation exists between these two. Therefore, since a correlation also exists between the engineering curve and the deformed shape, then the hardening law and the deformed shape are correlated too.

To better explain and show the correlation among the hardening law, the engineering curve and the deformed shape the authors performed a series of numerical simulations of tensile tests by using the explicit and non-linear FE code LS-DYNA. In Fig. 5, the sketch of the cylindrical dog-bone specimen is shown. To exploit the symmetries, just a quarter of the sample is modeled and 2D-axisymmetric shell elements with 1 integration point are used. The mid cross-section is properly constrained, and a prescribed velocity is applied to the nodes at the end of the specimen.

In this preliminary phase copper specimens were considered ($E = 110$ GPa and $\upsilon = 0.34$) and a simple power-law hardening behavior [42,43] was used:

$$\sigma_{eq} = K\varepsilon_{eq.pl}^N \tag{9}$$

where K and N are the material model parameters. The reference hardening parameters are: $K = 400$ MPa, whereas different values of N (from 0.1 to 0.6) are analyzed. As stated in Section 1, the influence of strain-rate and temperature are considered negligible.

According to Eq. (2), the instability strain is directly represented by the exponent N. Thus, as shown in Fig. 6a the model with $N = 0.6$ exhibits a long phase characterized by uniform elongation, while the model with $N = 0.1$ necks almost immediately after the yielding. The different duration of the pre-necking phase causes a different reduction of the diameter before necking onset: the diameter of the portion of specimen just outside the necking region is smaller for a model with smaller N (see Fig. 6b).

2.2. The algorithm

As already mentioned, FE-based inverse numerical methods directly compare experimental and numerical results on the basis of specific objective (or target) functions.

In the proposed strategy the comparison is done in terms of radial displacement Δr between the original configuration and the deformed one, identified by the axial displacement ΔL of a particular point, called "reference point/node".

More specifically, the principle is the one briefly described below. At first, the hardening law is chosen, and first attempt parameters are defined, then an optimization code performs FE simulations and, when the axial displacement of the reference node is equal to the corresponding experimental one, the radial displacements obtained from the simulation are compared with the experimental measurements. If the difference is greater than the prescribed tolerance, another set of experiments will be performed until the desired accuracy, or the maximum number of iterations is achieved.
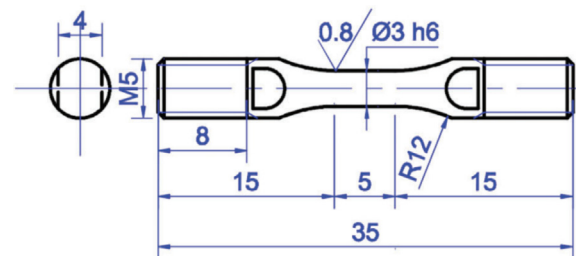

Fig. 5. Sketch of the cylindrical dog-bone specimen used in the numerical simulations of the tensile tests adopted by the authors in several testing campaigns [54].
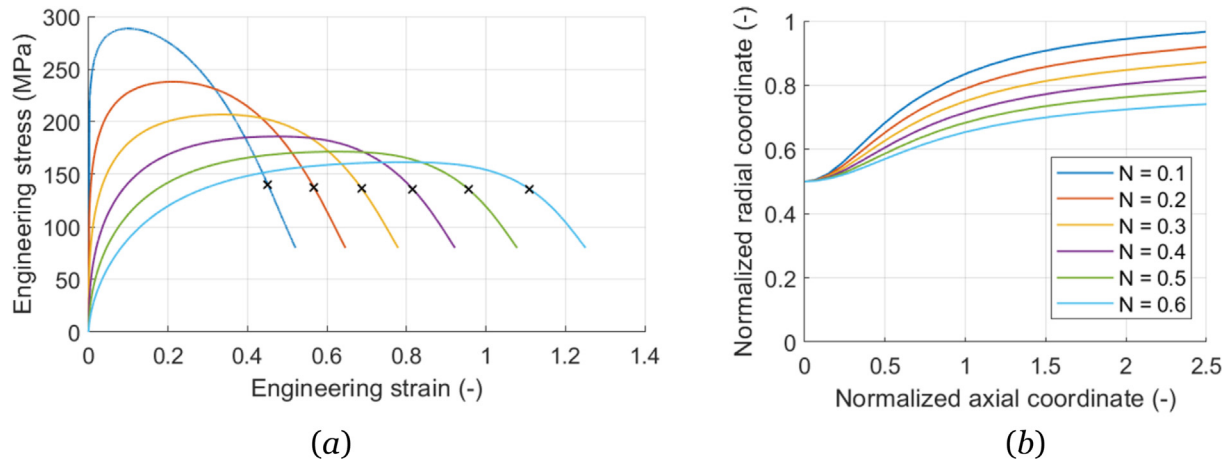
Fig. 6. Effect of a different exponent N of the power law plasticity model on the engineering curves (a) and on the specimen profiles (b). The profiles refer to deformed configurations that are characterized by the same minimum cross section and are marked with a cross in (a). The coordinates are normalized with respect to the initial radius.ρ.

This highlights that the essential aspects of the proposed methodology are:

- the construction of a parameterized FE model to be used within the optimization, which simulates the tensile test properly without requiring high computational time;
- the definition of the target functions, starting from experimental results, and of the data to be extracted from the simulation.

2.2.1. Construction of the FE model

First of all, it is necessary to realize a FE model that mimics a quasi-static tensile test in which the instability condition is reached. Since high levels of strain are achieved, a non-linear FE analysis must be performed; thus, it is required to use a proper code and the general-purpose software LS-DYNA is chosen.

Moreover, it is essential to save CPU and time in the numerical calculations, especially because of the iterative optimization procedure required in the inverse approach.

Therefore, as already outlined, the choice of referring to a dog-bone cylindrical specimen allows to exploit the symmetries and to use a 2D axisymmetric model of just a quarter of the sample.

Furthermore, the high level of deformation developed during necking requires techniques capable of limiting the elements' distortion. The solution adopted is to employ a coarse model with variable mesh, as shown in Fig. 7.

Additional analyses were carried out in order to study different possible solutions that may allow to save computational time, e.g., using under-integrated elements, increasing the test speed with respect to the experimental one, exploiting the selective mass-scaling technique or simulating only a portion of the specimen. Except for this last strategy (that shows no advantages with

respect to the others when the ratio $L/2\rho$ is lower than 2), all the other techniques contribute to reduce the computational effort without affecting the results in terms of force vs. stroke curve and deformed shape of the specimen. If an explicit solver is used, the previous considerations are true provided that no inertial effect is introduced. However, in a general case, which of these strategies can be adopted to reduce computational time and to which amount it is possible to exploit each of them depends on the specific situation (e.g., stress state, material law, slenderness ratio, etc.). Hence, once a first estimate of the material parameters is obtained, it is necessary to check that the simplifications introduced do not significantly affect the results; otherwise, the identification must be repeated using different modeling choices, so that better results are obtained, implying on the other hand higher computational time.

2.2.2. Definition of targets

To implement the optimization required by the proposed method it is necessary to assign a target to all or just some of the nodes of the FE model that are on the specimen surface and within the gauge length. As previously said, this target is the radial displacement of the specific node at a given axial displacement of a reference node. Therefore:

● from experimental data, it is required to determine both the radial displacement of the point corresponding to the specific node and the axial displacement of the point corresponding to the reference node;
● from FE simulation (at each iteration), it is required to extract the time history of both the radial displacement of the specific node and the axial displacement of the reference node.

For each node that is of interest, the optimization aims to obtain that the radial displacement of the node itself as function of the axial displacement of the reference node passes through the target experimental point.

The experimental values of the radial displacement Δr can be easily determined starting from the measured profile. For the points inside the gauge length $\Delta r(x) = r(x) - \rho$ and these values are the ones to be used as targets.

To properly define the target functions, it is required to know the axial position of each node in the deformed configuration that is of interest, in order to find which radial displacement experimentally measured must be assigned as target to that particular
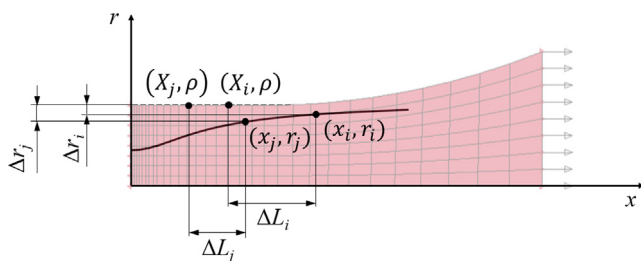

Fig. 7. Scheme for the target definition: correlation between the reference and the deformed configurations in terms of points coordinates.

node. Therefore, a relationship between the position of the nodes in the original configuration and their position in the deformed configuration is needed. This is provided by the 1D model proposed in [2], especially by kinematic results reported in Eq. 5, as already described.

At first, it is necessary to estimate the initial axial position $\bar{X}_i$ of some sampling points (x_i, r_i) measured on the profile. So, Eq. (5a) must be inverted and λ must be determined.

Starting from Eq. (5b) it is possible to estimate the axial stretch λ_i, on the basis of the measurement of the profile:

$$\lambda_i = \left(\frac{\rho}{r_i}\right)^2. \tag{10}$$

Indeed, it has been verified using FE simulations that the axial stretch computed through Eq. (10) adequately approximates the one computed through the definition given in Eq. (3).

However, the stretch obtained is a function of the deformed axial coordinate x and not of the initial axial coordinate X; therefore, an iterative procedure is required to solve Eq. (5a). The principle is to find the initial axial coordinate of the sampling points so that the deformed axial coordinate $\bar{x}_i$ obtained through Eq. (5a) is as close as possible to the experimental values x_i.

It is thus possible to create a FE model with nodes in the axial positions $\bar{X}_i$ that have been computed, so that the target displacements to assign are known. On the other hand, this would require a different mesh for each experimental test: indeed, since each test gives a different profile, a different original position of the same sampling point would be obtained.

However, once the initial position of the sampling points is computed, $\lambda(X)$ is known and it is possible to determine the deformed position of any point in the original configuration by means of Eq. (5a). Hence, it is convenient to consider a fixed mesh and compute the position of the nodes on the necking profile. In this way, the axial position of each node in the deformed configuration is known and the corresponding target displacements are taken from the experimental profile.

Simultaneously it is also possible to determine the axial displacement of these nodes and one of them is chosen as reference node (preferably the one that is furthest from the minimum cross-section).

In this way all the required information for the definition of the targets is obtained. In general, since the nodes outside the necking region experience only uniform deformation, they give information about incipient necking strain, but not about the post-necking behavior. Therefore, the target can be represented by all the nodes in the necking region and only few located outside.

The accuracy of the described computation will be verified in the numerical validation presented in Section 3 and will allow to evaluate the overall effect of the approximations intrinsic in the 1D model and of violating some hypotheses of the 1D theory.

For example, the main issue related to the use of Eq. 5 for studying the necking phenomenon in elasto-plastic materials is that it is derived for a hyperelastic material. On one hand, a nonlinear elastic model is widely used to study elasto-plastic materials if the strains increase monotonically, on the other hand the response of such materials is very different when the stretch decreases. Since during necking the localization of the deformation causes the stretch to increase in a limited region and to decrease elsewhere, the evolution of this phenomenon is significantly different in a nonlinear elastic material and in an elasto-plastic material. In the first case, the unloading of the material outside the necking region provides the energy to deform the necking region itself; in the second case the energy release is much lower, due to the rigid elastic response of the material (the so-called "elastic unloading") [2].

Despite the fact that this affects the response of the material (so how $\lambda(X)$ changes in time), the accuracy of Eq. 5 is not compromised. This can be understood by considering that the effect of the elastic unloading is of the order of elastic deformations that are usually much smaller than the plastic ones. Furthermore, this will be verified by means of FE simulations that take into account also the complete unloading that occurs at the end of a tensile test. Thus, it can be concluded that the progressive unloading which occurs during the tensile test after the necking onset does not affect the validity of Eq. 5. Another aspect that may affect the validity of the described approach is that, even though the procedure is applied only to those points that are within the gauge length of the dog-bone specimen, the difference in the geometry (connections and finite aspect-ratio) with respect to the hypothesis of the 1D theory may have an effect.

However, the accuracy of the results will show that the overall effect of these aspects is acceptable.

3. Numerical validation

To test the validity and reliability of the proposed methodology, benchmark cases were considered by creating ad-hoc experimental profiles obtained via numerical simulations of a tensile sample (see Fig. 5) with different known power-law material models. A uniform and very fine mesh was used to avoid too high element deformation and distortion during post-necking [53]. Once the simulations had been performed, the specimen profiles (i.e., the coordinates of the nodes on the external surface) and the force vs. stroke curves were taken from the output database and they were considered as the results of ideal experimental tests. The results extracted from the numerical simulations are shown in Fig. 6.

On the basis of what observed in Section 2.2, some points on the profile were taken as sampling points and λ_i was determined starting from their radial position r_i in the deformed configuration according to Eq. (10). Then, by means of an iterative procedure implemented in MATLAB an approximation $\bar{X}_i$ of their original axial position was determined.

Thanks to the fact that the chosen sampling points (x_i, r_i) were actually nodes of the FE model, the estimated initial position $\bar{X}_i$ could be compared with the actual one X_i.

The results are shown in Fig. 8, where the error on $\times$ (that is actually the variable that the iterative procedure aims to minimize) is computed as $\left\|\frac{x-\bar{x}}{x}\right\|_2$ and the error on X computed as $\left\|\frac{X-\bar{X}}{X}\right\|_\infty$.

Of course, a small error on the estimate of x implies a larger error on X; this quantifies the level of approximation of both the 1D theory and the numerical computation of derivatives and integrals that are required within the iterative procedure.

Despite these results refer to a certain configuration, this analysis was carried out at other levels of deformation too. This showed that the error increases at higher levels of deformation. However, when very high levels of strain are reached, even FE are no more representative of the real behavior, not only because of the distortion of the mesh (which could be quite easily solved, even if with a greater computational effort), but above all because the ductile damage, that actually arises, is not modeled. Therefore, at the deformation levels of interest, the results obtained with the 1D theory are considered sufficiently accurate (also taking into account that additional errors could have been introduced in this study due to the use of first-order numerical derivation formulas).

Thanks to the outlined procedure, $\lambda(X)$ was known, so it was possible to determine the deformed axial coordinate of any point of the reference configuration. Hence, a FE model of the specimen was built and the deformed axial position x_q of its nodes (in the

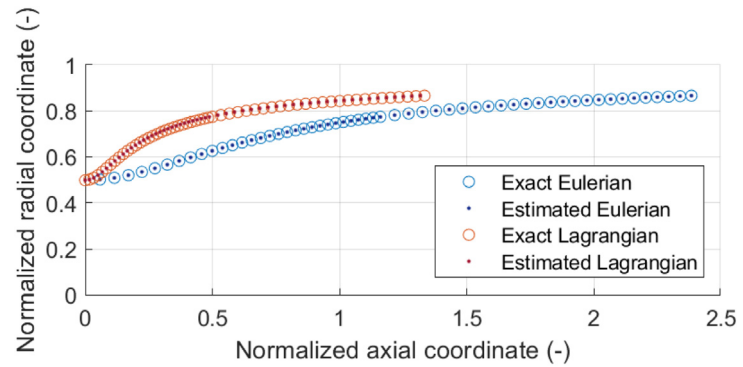| N	Error on x	Error on X
0.1	0.042%	2.42%
0.2	0.039%	1.80%
0.3	0.046%	1.27%
0.4	0.030%	0.88%
0.5	0.033%	0.59%
0.6	0.041%	0.44%

Fig. 8. Results of the iterative procedure to determine the initial position of some sampling points. The table presents the error on x and the error on X. The plot shows the following profiles for the case N = 0.3: exact Eulerian (x_i, r_i), estimated Eulerian $(\bar{x}_i, r_i)$, exact Lagrangian (X_i, r_i), estimated Lagrangian $(\bar{X}_i, r_i)$; the coordinates are normalized with respect to the initial radius ρ.

deformed configuration that is of interest) could be estimated; thus, the corresponding target radial displacements Δr_q could be taken from the experimental profile. Moreover, the extreme node could be chosen as the reference node for the axial displacement as required for the definition of the target functions previously described.

In this way all the required information to correctly define the targets was obtained.

The following step was to determine the plastic flow curve that would allow to obtain the target specimen shape. This was actually a problem of parameter identification which requires an optimization procedure. Thus, the commercial program LS-OPT was chosen: by the parameterized simulation of the tensile tests with LS-DYNA, it performs an automated calibration to the experimental results. In particular, a metamodel-based optimization was employed: a linear metamodel was used and for its automatic optimization the sequential strategy with domain reduction was exploited, whereby the point selection was performed according to the D-optimal strategy. Moreover, at the end of the last iteration, a verification run of the predicted optimal parameters is executed.

As already stated in Section 2.2 "Construction of the FE model", it is important for the FE model used within the optimization to have a limited computational time, so a coarse mesh (as the one shown in Fig. 7) was used and the selective mass-scaling strategy was employed.

The results presented in Fig. 9 allow to evaluate the capability of the proposed method to identify the plastic flow curve of a ductile material. The error on N is evaluated by dividing the difference between the expected value and the optimum one $(\bar{N})$ for the expected value. The error on the profile is presented too and is computed as the root mean square error between the target profile and the one obtained with the identified hardening law. Moreover, in the plot of Fig. 9 the prediction of the necking onset is compared with the actual necking onset; also the prediction of the maximum equivalent plastic strain reached inside the specimen at the deformed configuration considered as target is compared with the actual one.

The optimization converged to a value of N which differed from the expected one by 3.4% in the worst case. However, Fig. 9 shows that it is almost impossible to appreciate this difference in the plastic flow curve. The difference between the target specimen shapes and the ones obtained with the identified hardening laws was also evaluated. Moreover, the authors performed FE simulations that take into account also the complete unloading that occurs at the end of a tensile test and observed that the deformed shape just before and after the unloading are very close to each other, with

a root mean square error of $1.85 \cdot 10^{-3}$ mm in the worst case. This means that the progressive unloading which occurs during the tensile test after the necking onset does not affect the validity of Eq. 5, as already discussed in Section 2.2 "Definition of targets".

In conclusion, on the basis of the tests performed, it is possible to state that all the steps that exploit the 1D theory do not introduce significant errors. Furthermore, it was shown that limited inertial effects do not significantly alter the results.

Of course, knowing the material a priori, it was possible to quantify the effect of inertia, whereas in an experimental case, once the hardening parameters have been identified, it is necessary to check that the strategies adopted to reduce the computational effort do not affect the results. Moreover, the plastic flow curve is generally more complex than a power-law and so it is important to adequately choose a hardening model and it may be necessary to assign an objective function to a number of nodes higher than those considered here. However, not having in the numerical validation these variables, it was possible to evaluate the accuracy of the proposed method itself.

4. Case study

In this paragraph a case study for the experimental application of the proposed method is presented. The aim is verifying its effectiveness and comparing this strategy with a traditional approach whereby the force vs. stroke curve is used as target.

Reference was made to already available experimental data of quasi-static tensile tests (in which the material was not brought to fracture) carried out on pure copper specimens, one of which was previously annealed (550 °C/2h); the geometry is shown in Fig. 5. The available data were the force measured by a load cell and the video of the test, made with a high-resolution camera.

The annealing causes the behavior of the two samples to be significantly different, therefore the methodology was tested on two very different behaviors: in the annealed specimen the necking onset occurred after large uniform plastic deformation, whereas in the other specimen it occurred shortly after the deviation from linearity.

The proposed methodology and the traditional one were implemented; however particular care was required both in building a FE model (to be used in optimization) and in defining the objective functions. For what FE simulations are concerned, all the material data were assumed *a priori*, except for the hardening law (which instead required adequate parameterization) and the FE model was common to both methodologies (and the one shown in Fig. 7), whereas of course the objective functions are different, and it was thus necessary to cope with different issues.

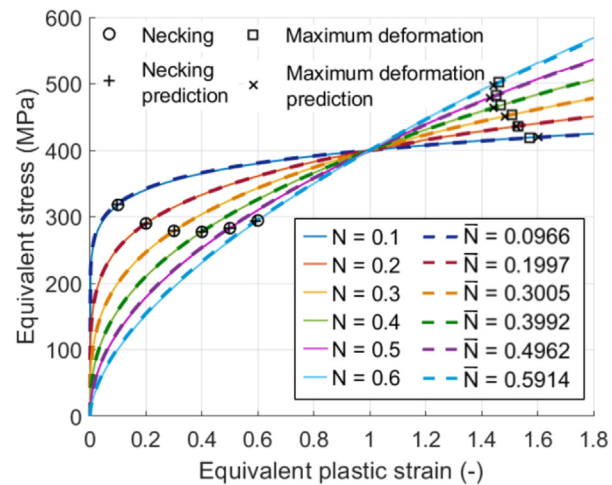| N expected	$\overline{N}$ optimum	Error on N	Error on the profile (mm)
0.1	0.0966	3.41%	0.0034
0.2	0.1997	0.16%	0.0018
0.3	0.3005	0.17%	0.0037
0.4	0.3992	0.19%	0.0042
0.5	0.4962	0.77%	0.0039
0.6	0.5914	1.43%	0.0032

Fig. 9. The table compares the expected value of N with the optimum one $\overline{N}$ identified by the proposed method; it also presents the error on the profile. In the plot dashed lines represent the plastic flow curve identified by the proposed method whereas continuous lines represent the plastic flow curve used to numerically generate the target profile; the actual necking onset and the actual maximum deformation are compared with the prediction done through the identified hardening law.

4.1. Material data and parameterized hardening law

For what material data is concerned, reference was made to the values used in Section 2.1.

The hardening model is defined through parameters that were identified using the proposed and traditional methods; however, it was also necessary to choose the mathematical law. Different models were used to evaluate which was more representative of the behavior of the specific materials, in particular power law [42,43], Johnson-Cook [44] and Voce [45] hardening models were considered. However, none of them proved to adequately describe the behavior of the considered materials.

Therefore, the possibility of using a piecewise linear hardening law was studied (as already done in [30,36,46,47]). Indeed, being defined by points, it is not bound to a specific mathematical relationship and, therefore, potentially allows a better description of the behavior of the material (implemented in LS-DYNA as *MAT-024). All the points of the hardening law that can be obtained experimentally, so up to the necking onset, were computed analytically. The following points, instead, were defined by means of parameters: $\varepsilon_{eq,pl}$ was fixed and the corresponding values of σ_{eq} were defined through parameters which represented the optimization variables. The parameterization was such that the hardening curve was monotonically increasing with decreasing derivative, as generally occurs in metals. It was also necessary to ensure that the last points of the plastic flow curve just before necking were such to satisfy Considère criterion, in this way necking occurred in the model at the same elongation at which it happened in the experimental test.

4.2. Proposed methodology: experimental profile as objective function

The profile within the gauge marks is used as an objective function. This was experimentally determined by Digital Image Analysis of a frame in which the specimen had reached a high level of post-necking deformation. The frame considered was the one where half the elongation of the gauge length was δ_*^{na} and δ_*^{a} respectively for the non-annealed and the annealed specimens (see Fig. 11).

The obtained profile was filtered to reduce the noise level and to neglect the non-physical oscillations. Furthermore, since the image was the full specimen, the ideal symmetry and equivalence of the four semi-profiles was exploited, thus computing an average semi-profile with lower noise [53].

The method proposed in this paper requires taking some sampling points on the average semi-profile and computing their original position. To avoid taking into account points outside the gage length, it was necessary to verify that all the initial coordinates were at a distance lower than 2.5 mm from the minimum section; otherwise, those outside this range must not be taken into account.

Having determined the initial position of the sampling points, the function $r(X)$ (i.e., a sort of "Lagrangian profile") can be represented as shown in Fig. 10.

Then it was possible to determine the position on the deformed profile of the nodes of the FE model used for the optimization; thus, the radial displacement of these points could be assigned to the nodes as target.

Furthermore, to properly define the target it is necessary to choose a reference node too. In particular, the choice was to consider as reference node the one that was farthest from the minimum cross-section and for which it was possible to calculate the axial position (and so the axial displacement) in the deformed configuration.

4.3. Traditional approach: experimental force vs. elongation curve as objective function

The force vs. elongation curve used as objective function was referred to the gauge marks for the measurement of the elongation. So, it was necessary to use Digital Image Analysis to determine the experimental displacement of these points.

Furthermore, it was required for the FE model to have a node in the position corresponding to the gauge marks; this was considered to be half of the initial distance between the gauge marks even if necking did not actually take place in the center of the specimen.

The decision to refer to these points rather than to the shoulders was due to the fact that the shoulders represent the extreme part of the FE model and are not constrained in any way, whereas the specimen heads, thread, etc. can introduce effects not taken into account by the model.

Finally, the portion of the force vs. stroke curve used as target was just the one in which a deviation from linearity is evident, i.e. the portion in which the material is certainly in the plastic field (above 2000 N in the non-annealed case and 400 N in the annealed
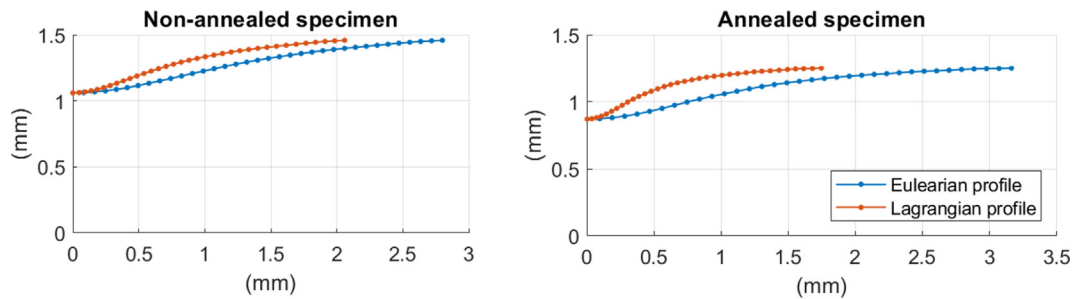
Fig. 10. Eulerian and Lagrangian profile at δ_*^{na} for the non-annealed specimen and at δ_*^a for the annealed one. The ordinate is the radial coordinate r, whereas the abscissa is the axial coordinate x for the Eulerian profiles and X for the Lagrangian profiles.

case). Moreover, to get results comparable with the proposed method, the force vs. stroke curve was considered as the target only up to $\delta = \delta_*^{na}$ for the non-annealed sample and $\delta = \delta_*^a$ for the annealed sample.

4.4. Results

As already stated, none of the identified hardening laws (power-law [42,43], Johnson-Cook [44], Voce [45]) was able to properly catch the behavior of these materials. However, using models with a specific mathematical relationship, does not allow to understand if the discrepancy between the optimum solution and the experimental result is due to the hardening model or to the methodology itself. So, a piecewise linear hardening model was considered. The points before the necking onset were determined analytically so that the necking onset was correctly predicted. This would not occur with a mathematical relationship, unless the optimization was properly conditioned.

The results are shown in Fig. 11a in terms of force vs. stroke curve and in Fig. 11b in terms of specimen profile.

It is possible to note the great difference between the two materials' behavior. Indeed, the annealed specimen is much more ductile: the elongation reached when the test was interrupted is two times higher than in the other specimen. Of course, also the semi-profiles shown in Fig. 11b highlight the fact that the annealed specimen reached higher elongations: the radial contraction is greater than for the other specimen.

It can be seen that, for both inverse numerical methods, the identified hardening law allows to well reproduce the relative objective function. This is particularly important for the method based on the comparison of the profile, as it validates the procedure (see in Fig. 11b the shapes at $\delta = \delta_*^{na}$ for the non-annealed sample and at $\delta = \delta_*^a$ for the annealed sample). Indeed, if the steps performed were not adequate (especially those with the 1D theory), the resulting profile would not copy the experimental one.

Moreover, Fig. 11b also compares experimental and predicted specimen shapes at other three levels of deformation, different with respect to the level of deformation used as target. An estimation of the equivalent strain that characterizes each configuration can be found as $\bar{\varepsilon}_{eq} = \ln(\rho/r_{min})$. Therefore, $\bar{\varepsilon}_{eq,1}^{na} = 0.22$, $\bar{\varepsilon}_{eq,2}^{na} = 0.28$, $\bar{\varepsilon}_{eq,*}^{na} = 0.35$, $\bar{\varepsilon}_{eq,3}^{na} = 0.43$ for the non-annealed sample and $\bar{\varepsilon}_{eq,1}^{a} = 0.38$, $\bar{\varepsilon}_{eq,2}^{a} = 0.46$, $\bar{\varepsilon}_{eq,*}^{a} = 0.54$, $\bar{\varepsilon}_{eq,3}^{a} = 0.65$ for the annealed sample.

So, taking into account that the levels of deformation differ by 6–9% one with respect to the other, the agreement between the specimen shape is quite good. The results may be improved through a multi-objective optimization, where more than one post-necking deformed shape is used as target.

It can be noticed that when the force vs. elongation curve was used as target, the resulting profile differed from the experimental one and, *vice versa*, when the profile was used as target, the force vs. elongation curve did not match with the experimental one.

Therefore, to compare the two methods it is meaningful to look at the identified hardening laws (Fig. 12a).

A good agreement can be observed between the two solutions, with an average difference of 1.4% and 2.2% respectively for the case of annealed and non-annealed specimens.

As said in Section 2.2 "Construction of the FE model", it was also verified that these discrepancies had not been introduced by the choices made in modeling the tests in order to reduce the computational time of FE simulations.

Therefore, the difference between the identified hardening laws may be due to experimental errors and to additional variables that have not been considered. The first aspect is above all linked to the measurement of the displacements, to the determination of the specimen profile, and to the synchronization between the testing machine and the video camera. The second aspect includes, for example, the high strain-rates reached in the necking region and the fact that the minimum cross-section was not in the center of the specimen, as assumed in the FE model used within the optimization.

So, the comparison of the two identified hardening laws allows to estimate the effect that the experimental uncertainties and hypotheses adopted in modeling the tensile test have on the identification of the plastic flow curve. The results obtained show that this effect is rather limited in this case study, also considering that, from the point of view of an experimental campaign performed to characterize a material, the difference between experimental tests is probably greater than that obtained between the two methodologies.

Finally, it is possible to conclude that the method proposed in this paper provides results comparable to those of a traditional strategy based on the comparison of the force vs. elongation curve. On the other hand, it cannot be stated that one of the two methods leads to better results than the other, so the materials' behavior can be considered well described by a hardening law which is the average of the two identified.

From the plot of Fig. 12a it can also be noted that the instability is reached at almost the same stress in both samples: indeed, both specimens are made of copper, but the non-annealed one behaves as if it started from the last 1% of uniform deformation of the annealed sample. This can be understood by considering that the annealing "cancels" all the deformation history, but the material has the same possibilities of reaching the same stress values. This is also the reason why the two specimen shapes in the necking region are very similar if properly scaled so that the diameters outside the necking region are the same (Fig. 12b).
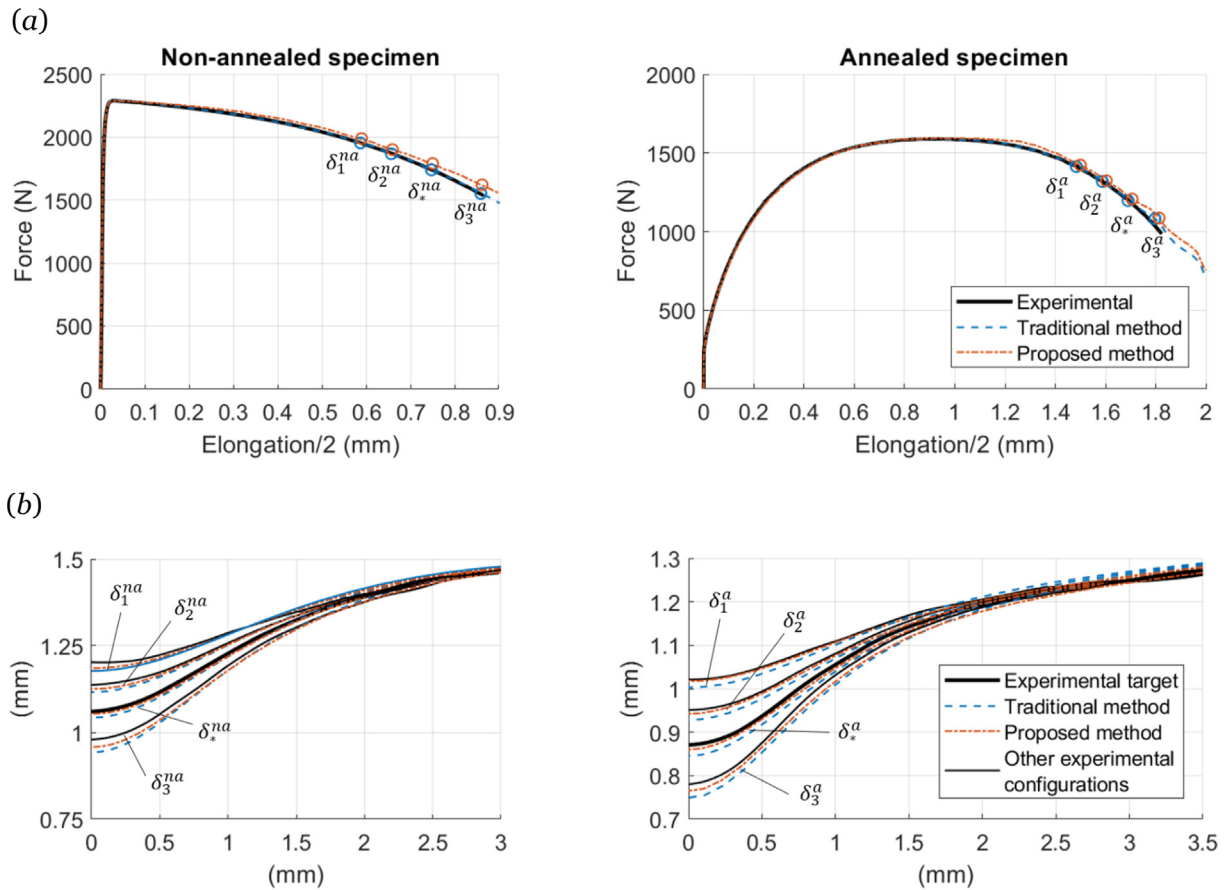
(a)

(b)

Fig. 11. Results of the traditional approach and the proposed method in case of linear piecewise plasticity for both the samples. (a) Comparison of the force vs. stroke curve. (b) Comparison of the experimental and predicted specimen profile at different time instants.
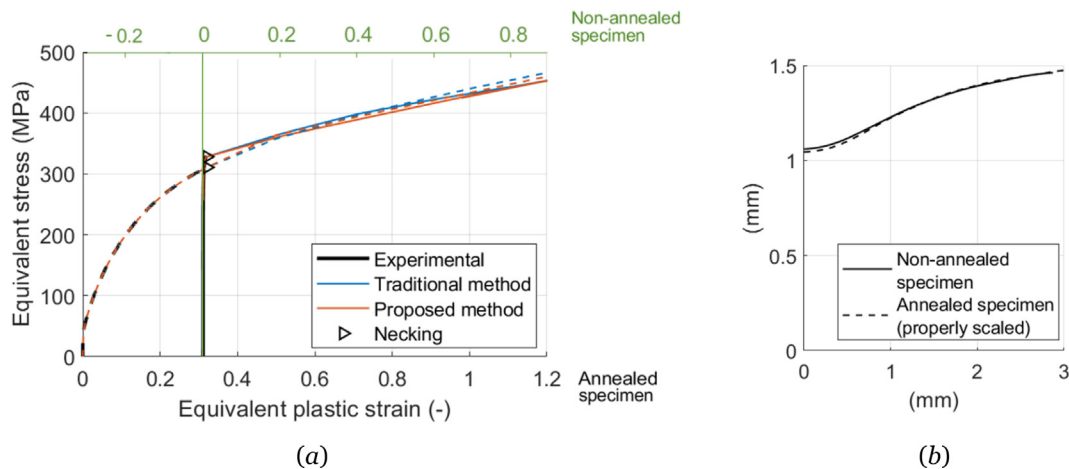

(a) (b)

Fig. 12. (a) Plastic flow curve identified with the two different approaches for both the samples: continuous lines refer to the non-annealed specimen whereas dashed lines refer to the annealed one. (b) Comparison of the deformed shape of the two samples by properly scaling the annealed specimen shape.

5. Conclusions

The aim of this work was to propose a methodology based on the analysis of the necking profile for the identification of elasto-plastic material models. This is actually a hybrid method which combines the numerical inverse procedure based on FE analysis with the kinematic results of Audoly and Hutchinson's 1D theory [2].

The proposed strategy was numerically validated and proved to be adequate also for experimental application. Indeed, in the presented case study, it allowed to obtain a hardening law close to the one resulting from a traditional inverse numerical method and such that the resulting profile was in very good agreement with the experimental one.

This analysis also highlighted the advantages and disadvantages of the two methods. The classical one is characterized by a lower

computational effort, but it requires particular considerations depending on the specific case and a careful analysis in modeling the constraints. Instead, the proposed strategy, even if more complex and computationally expensive, is applicable to different cases without requiring particular adjustments for both the FE model and the elaboration of the experimental data. In addition, the proposed method could be used to obtain information about the hardening law of the material starting from a post-mortem analysis of the specimen profile in the necking region.

Furthermore, regardless of the identification method used, it was shown that a valid alternative to the hardening models available in literature is represented by a piecewise linear curve, where the part preceding the necking onset is directly obtained from experimental data, while the following one must be identified.

Finally, it was also highlighted the potential of combining an inverse numerical method based on the comparison of the force vs. elongation curve with one based on the comparison of the profile. Both methodologies identify a plastic flow curve, and each of the latter is characterized by a certain error (due for example to experimental uncertainties and neglected variables in modeling the tensile test and/or the material). However, it is not possible to state that one result is better than the other and taking an average hardening law can be considered more reliable. In addition to a higher reliability, the combination of the two methodologies may allow to detect if some neglected variables (for example, strain-rate or ductile damage) play a significant role. Although a deduction of this type is also possible using just the traditional method and comparing the profile *a posteriori*, it would not be possible to evaluate the difference between a hardening law which allows to properly describe the force vs. stroke curve and one which allows to adequately reproduce the profile. Moreover, when additional parameters must be introduced to take into account strain-rate, ductile damage, etc., using different and independent methods to calibrate the model certainly gives more reliable results.

Data availability

Data will be made available on request.

Declaration of Competing Interest

The authors declare that they have no known competing financial interests or personal relationships that could have appeared to influence the work reported in this paper.

References

[1] J.W. Hutchinson, J.P. Miles, Bifurcation analysis of the onset of necking in an elastic/plastic cylinder under uniaxial tension, J. Mech. Phys. Solids 22 (1) (1974) 61–71.

[2] B. Audoly, J.W. Hutchinson, Analysis of necking based on a one-dimensional model, J. Mech. Phys. Solids 97 (2016) 68–91.

[3] Y. Yan, M. Li, Z.L. Zhao, X.Q. Feng, An energy method for the bifurcation analysis of necking, Extreme Mech. Lett. 101793 (2022).

[4] S. Coppieters, S. Cooreman, H. Sol, P. Van Houtte, D. Debruyne, Identification of the post-necking hardening behaviour of sheet metal by comparison of the internal and external work in the necking zone, J. Mater. Process. Technol. 211 (3) (2011) 545–552.

[5] M.K. Gupta, N.K. Singh, Post Necking Behaviour and Hardening Characterization of Mild Steel. In Solid State Phenomena vol. 319 (2021) 7–12.

[6] L. Zhu, X. Huang, H. Liu, Study on constitutive model of 05Cr17Ni4Cu4Nb stainless steel based on quasi-static tensile test, J. Mech. Sci. Technol. 36 (6) (2022) 2871–2878.

[7] P.W. Bridgman, Studies in Large Plastic Flow and Fracture. Metallurgy and Metallurgical Engineering Series, McGraw Hill, New York, 1952.

[8] M. Gromada, G. Mishuris, A. Öchsner, Correction Formulae for the Stress Distribution in Round Tensile Specimens at Neck Presence, Springer Science & Business Media, 2011.

[9] G. Le Roy, J.D. Embry, G. Edwards, M.F. Ashby, A model of ductile fracture based on the nucleation and growth of voids, Acta Metall. 29 (8) (1981) 1509–1522.

[10] E.E. Cabezas, D.J. Celentano, Experimental and numerical analysis of the tensile test using sheet specimens, Finite Elem. Anal. Des. 40 (5–6) (2004) 555–575.

[11] G. Mirone, A new model for the elastoplastic characterization and the stress–strain determination on the necking section of a tensile specimen, Int. J. Solids Struct. 41 (13) (2004) 3545–3564.

[12] G. Mirone, D. Corallo, Stress–strain and ductile fracture characterization of an X100 anisotropic steel: experiments and modelling, Eng. Fract. Mech. 102 (2013) 118–145.

[13] G. Mirone, D. Corallo, R. Barbagallo, Experimental issues in tensile Hopkinson bar testing and a model of dynamic hardening, Int. J. Impact Eng 103 (2017) 180–194.

[14] J.M. Choung, S.R. Cho, Study on true stress correction from tensile tests, J. Mech. Sci. Technol. 22 (6) (2008) 1039–1051.

[15] S. Tu, X. Ren, J. He, Z. Zhang, A method for determining material's equivalent stress-strain curve with any axisymmetric notched tensile specimens without Bridgman correction, Int. J. Mech. Sci. 135 (2018) 656–667.

[16] Y.Z. Wang, G.Q. Li, Y.B. Wang, Y.F. Lyu, Simplified method to identify full von Mises stress-strain curve of structural metals, J. Constr. Steel Res. 181 (2021) 106624.

[17] A. Mielke, Hamiltonian and Lagrangian Flows on Center Manifolds: With Applications to Elliptic Variational Problems, Springer-Verlag, 1991.

[18] B. Audoly, J.W. Hutchinson, One-dimensional modeling of necking in rate-dependent materials, J. Mech. Phys. Solids 123 (2019) 149–171.

[19] M. Dunand, D. Mohr, On the predictive capabilities of the shear modified gurson and the modified Mohr-Coulomb fracture models over a wide range of stress triaxialities and lode angles, J. Mech. Phys. Solids 59 (7) (2011) 1374–1394.

[20] M. Scapin, L. Peroni, M. Peroni, Parameters identification in strain-rate and thermal sensitive visco-plastic material model for an alumina dispersion strengthened copper, Int. J. Impact Eng 40 (2012) 58–67.

[21] C.C. Roth, D. Mohr, Determining the strain to fracture for simple shear for a wide range of sheet metals, Int. J. Mech. Sci. 149 (2018) 224–240.

[22] Z. Yao, W. Wang, Full-range strain-hardening behavior of structural steels: Experimental identification and numerical simulation, J. Constr. Steel Res. 194 (2022) 107329.

[23] X. Zeng, J.S. Huo, Rate-dependent constitutive model of high-strength reinforcing steel HTRB600E in tension, Constr. Build. Mater. 363 (2023) 129824.

[24] Z. Shokeir, J. Besson, C. Belhadj, T. Petit, Y. Madi, Edge tracing technique to study post-necking behavior and failure in Al alloys and anisotropic plasticity in line pipe steels, Fatigue Fract. Eng. Mater. Struct. 45 (9) (2022) 2427–2442.

[25] N. Bonora, A. Ruggiero, P.J. Flater, J.W. House, R.J. DeAngelis, On the Role of Material Post-Necking Stress-Strain Curve in the Simulation of Dynamic Impact vol. 845, No. 1 (2006) 701–704.

[26] M. Scapin, L. Peroni, C. Fichera, A. Cambriani, Tensile behavior of T91 steel over a wide range of temperatures and strain-rate up to 104 s^{-1}, J. Mater. Eng. Perform. 23 (8) (2014) 3007–3017.

[27] M. Scapin, L. Peroni, F. Carra, Investigation and mechanical modelling of pure molybdenum at high strain-rate and temperature, J. Dynam. Behav. Mater. 2 (2016) 460–475.

[28] M. Scapin, L. Peroni, C. Torregrosa, A. Perillo-Marcone, M. Calviani, L.G. Pereira, Experimental results and strength model identification of pure iridium, Int. J. Impact Eng 106 (2017) 191–201.

[29] M. Scapin, L. Peroni, C. Torregrosa, A. Perillo-Marcone, M. Calviani, Effect of strain-rate and temperature on mechanical response of pure tungsten, J. Dynam. Behav. Mater. 5 (3) (2019) 296–308.

[30] S. Marth, H.-Å. Häggblad, M. Oldenburg, R. Östlund, Post necking characterisation for sheet metal materials using full field measurement, J. Mater. Process. Technol. 238 (2016) 315–324.

[31] J.R. Li, G.B. Yang, T. Siebert, M.F. Shi, L. Yang, A method of the direct measurement of the true stress-strain curve over a large strain range using multi-camera digital image correlation, Opt. Lasers Eng. 107 (2018) 194–201.

[32] Z. Xu, L. Peng, M.K. Jain, D. Anderson, J. Carsley, Local and global tensile deformation behavior of aa7075 sheet material at 673ok and different strain rates, Int. J. Mech. Sci. 195 (2021) 106241.

[33] E. Scharifi, T. Schade, A. Ademaj, S.V. Sajadifar, U. Weidig, T. Niendorf, K. Steinhoff, Characterization of mechanical properties, macroscopic deformation behavior, and microstructure of functionally graded 22MnB5 Steel, Steel Res. Int. 92 (7) (2021) 2000633.

[34] D. Yao, Y. Duan, Y. Guan, S. Pu, A forward identification method for high-temperature stress-strain curves of 7075 aluminum alloy sheet considering the necking stage, Materials 15 (20) (2022) 7093.

[35] B. Jordan, V. Grolleau, D. Mohr, Using surround DIC to extract true stress–strain curve from uniaxial tension experiments, Int. J. Solids Struct. 268 (2023) 112171.

[36] J. Kajberg, G. Lindkvist, Characterisation of materials subjected to large strains by inverse modelling based on in-plane displacement fields, Int. J. Solids Struct. 41 (13) (2004) 3439–3459.

[37] A.J. Gross, K. Ravi-Chandar, On the extraction of elastic–plastic constitutive properties from three-dimensional deformation measurements, J. Appl. Mech. 82 (7) (2015).

[38] H. Zhang, S. Coppieters, C. Jiménez-Peña, D. Debruyne, Inverse identification of the post-necking work hardening behaviour of thick HSS through full-field strain measurements during diffuse necking, Mech. Mater. 129 (2019) 361–374.

[39] S. Coppieters, K. Ichikawa, T. Kuwabara, Identification of strain hardening phenomena in sheet metal at large plastic strains, Procedia Eng. 81 (2014) 1288–1293.

[40] J.R. Zhong, T. Xu, K.S. Guan, J.A. Szpunar, An improved procedure for acquiring yield curves over a large range of strains, J. Strain Anal. Eng. Des. 54 (4) (2019) 227–235.

[41] Q.T. Pham, N.T. Trung, J.J. Ha, Y.S. Kim, Hybrid fitting-numerical method for determining strain-hardening behavior of sheet metals, Mech. Mater. 161 (2021) 104031.

[42] W. Ramberg, W.R. Osgood, Description of stress-strain curves by three parameters. Technical Report, NASA Science and Technical Information Facility, Technical Note No. 902, 1943.

[43] J.H. Hollomon, Tensile deformation. AIME Trans. 12 (4) (1945) 1–22.

[44] G.R. Johnson, W.H. Cook, A constitutive model and data for metals subjected to large strains, high strain-rates and high temperature, in: The 7th International Symposium on Ballistic, 1983, pp. 541–547.

[45] E. Voce, A practical strain hardening function, Metallurgia 51 (1955) 219–226.

[46] M. Dunand, D. Mohr, Hybrid experimental–numerical analysis of basic ductile fracture experiments for sheet metals, Int. J. Solids Struct. 47 (9) (2010) 1130–1143.

[47] L. Wang, W. Tong, Identification of post-necking strain hardening behavior of thin sheet metals from image-based surface strain data in uniaxial tension tests, Int. J. Solids Struct. 75 (2015) 12–31.

[48] G.H. Majzoobi, S.F.Z. Khosroshahi, H.B. Mohammadloo, Determination of materials parameters under dynamic loading: Part II: optimization, Comput. Mater. Sci. 49 (2) (2010) 201–208.

[49] G.H. Majzoobi, F. Fariba, M.K. Pipelzadeh, S.J. Hardy, A new approach for the correction of stress–strain curves after necking in metals, J, Strain Anal. Eng. Des. 50 (2) (2015) 125–137.

[50] A. Rezaei Pour Almasi, F. Fariba, S. Rasoli, Modifying stress-strain curves using optimization and finite elements simulation methods, J. Solid Mech. 7 (1) (2015) 71–82.

[51] A. Shahrjerdi, B. Ranjbar, Correction of post-necking stress–strain curve of copper using surface strain method, Arch. Appl. Mech. 92 (1) (2022) 199–219.

[52] A. Shahrjerdi, M.R. Dost Mohammadi, Correction of the stress–strain curve for 2024 aluminum alloy after necking using the new surface strain method, Proc. Inst. Mech. Eng. C J. Mech. Eng. Sci. 236 (15) (2022) 8582–8597.

[53] L. Peroni, M. Scapin, Strength Model Evaluation Based on Experimental Measurements of Necking Profile in Ductile Metals, EPJ Web of Conferences, vol. 183, EDP Sciences, 2018, p. 01015.

[54] M. Scapin, L. Peroni, C. Fichera, Investigation of dynamic behaviour of copper at high temperature, Mater. High Temp. 31 (2) (2014) 131–140.